7.2 IMPACTS OF FIRE/ATMOSPHERE COUPLING AND BOUNDARY–LAYER TURBULENCE ON FIREBRAND PROPAGATION

Mary Ann Jenkins[1] * Sangay Bhutia[1] and Ruiyu Sun[2]
[1]York University, Toronto, Canada
[2]UCAR and EMC/NCEP/NOAA, Camp Springs, MD

1. Introduction

The spread of wildland fire by windborne embers or firebrands is known as "spotting." Burning brands or embers, lofted above wildfires and carried by the turbulent flow, can land and cause spot ignitions far from the flame front. As a consequence of its highly uncertain nature and dependence on various vegetation and meteorological conditions, this mode of fire spread has proved to be a major problem to fire-fighters and their strategies.

Fire spread by brand spotting consists of three elements: lofting, propagation or transport, and deposition with fire ignition. From the moment it becomes airborne, a firebrand's trajectory depends on $\vec{V}$, the evolution of the three–dimensional, time-varying flow field that results from the interaction of the fire plume's convection with the Atmospheric Boundary Layer (ABL) flow. A numerical model capable of simulating all these elements of the event under various topographical, meteorological, and vegetative conditions would be invaluable in *a priori* development of fire–fighting strategies.

In Albini (1983)'s work on transport of firebrands by line thermals, the behavior of a strong line thermal was modeled, idealized as a well-mixed cylindrical structure, in a quiescent unstratified atmosphere. Then the trajectory of a firebrand particle having no aerodynamic lift was calculated assuming it to be inside the thermal. Finally, the downwind transport was superimposed, assuming that the thermal structure is embedded in, but not interacting with, a mean windfield described by a constant vertical velocity profile.

Fire brand models have continued to de-couple the lofting and propagation phases [e.g., Baum and McCaffrey (1989)] or to add simple combinations of fire plume and/or ambient winds [e.g., Tse and Fernandez-Pello (1998)]. These analyzes are restricted to two dimensions, the fires are idealized as stationary fires and the plume velocity field is described using a time-mean, plume–averaged steady vertical velocity field. Any interaction between the fire and the atmosphere is neglected. Although these models have not been rigorously tested or validated, they are widely used by fire behavior analysts in the United States and Canada (Alexander et al., 2004), where it is assumed that they predict the so–called "worst–case" scenario.

Despite the fact that much of the phenomenology of spotting is widely known, no previous model of fire propagation by brand spotting combines or couples all three elements or takes into account explicitly the effects of the turbulence in the flow associated with the wildfire and its environment. This is what this study attempts to do, and it shows that the lofting of firebrands in the non–steady background flow caused by the interaction of the fire-induced convection with the turbulence in the ABL is crucial to spot fire prediction.

Here we compare the lofting and propagation of spherical firbrands determined by two different numerical models. The first is a slightly modified version of the Baum and McCaffrey (1989) model and is presented in Section 2. Lofting and propagation of combusting and non-combusting firebrands by this simple modeling approach are used to examine the relationships between lofting height, propagation distance, and brand particle size. The analysis is restricted by the same set of assumptions used in current operational wildfire formulae and reflects the past efforts on operational spot fire modeling described in this section. The second model depicts the behavior and propagation of fire brands in a coupled fire/atmosphere wind field, and is presented in Section 2, where a fluid dynamical approach to the problem of spotting by firebrands is examined. Readers are referred to Bhutia et al. (2009) for further details. Combustion characteristics of firebrands, coupled with mass and size histories, are also required by fire propagation to calculate fire spotting distances. Mass loss rate and size regression of firebrands are determined by Tse and Fernandez-Pello (1998)'s firebrand combustion model adapted for our purposes. Spherical firebrands have no lift, and therefore they cannot glide. Only forces of drag and gravity act on a spherical firebrand. Again readers are referred to Bhutia et al. (2009) for details.

* *Corresponding author address:* Department of Earth and Space Science and Engineering, York University, Toronto, ON, Canada, M3J 1P3. E-mail: maj@yorku.ca

2. A Mean Plume Flow Field

The mean plume flow field above a single isolated fire is described using a slightly modified version of the Baum and McCaffrey (1989) plume model. This model assumes a stationary, buoyancy–driven fire burning at a constant rate in a quiescent neutrally–stratified ambient atmosphere. The fire is modeled as a typical pool fire of three reasonably distinct regions; Region I, the lowest region is the continuous burning zone, where flame sheets are anchored to the fuel bed and the flow is not steady but pulsates regularly; Region I, an intermittent zone, contains irregular patches of flame breaking off from the anchored flame; Region III, the plume region above the top of the visible flame zone where almost all combustion ceases, is characterised by classical velocity and thermal structure induced by a weakly buoyant source. The plume form makes maximum use of classical plume theory. It is assumed that the time–averaged vertical velocity and temperature rise in the central region of a buoyant plume have a Gaussian radial distribution (McCaffrey, 1983). The parameters of vertical distance z, plume velocity U_p, and temperature T are made dimensionless as follows:

$$\frac{z}{z_c} = z^*, \tag{1}$$

$$\frac{U_p}{U_c} = U_p^*, \tag{2}$$

and

$$\frac{(T - T_0)}{T_0} = T^* \tag{3}$$

where

$$z_c = \Big(\frac{\dot{Q}_0}{\rho_a c_p T_0 \sqrt{g}}\Big)^{2/5}, \tag{4}$$

and

$$U_c = \sqrt{g z_c}. \tag{5}$$

Here $\dot{Q}_0$ is the total heat release rate, g is the acceleration due to gravity, ρ_a is the density of the ambient air, c_P is the specific heat capacity of air at constant pressure, and T_0 is the temperature of the ambient air. The temperature and velocity correlations developed by McCaffrey (1983) provide that U_p^* and T^* are the following functions of z^* only:

$$U_p^* = A(z^*)^n, \tag{6}$$

$$T^* = B(z^*)^{2n-1}. \tag{7}$$

The quantities n, A, B for each region are given in Table 1. Figure 1a illustrates the vertical profile of the plume velocity U_p above a fire for total heat release rate $\dot{Q}_0$= 5.0 MW.

In the absence of an ambient wind field, the only motion possible in the interior of the plume is vertical. In this case, the equations governing the motion of particles reduce to

$$\frac{dV_{p,z}}{dt} = \frac{1}{2m_p} C_D \rho_a A_{proj} |\vec{V}_r| (W - V_{p,z}) - g. \tag{8}$$

Using the Baum & McCaffrey plume model to describe the plume velocity field, the above equation becomes

$$\frac{dV_{p,z}}{dt} = \frac{1}{m_p} C_D \rho_a A |\vec{V}_r| (U_p - V_{p,z}) - g, \tag{9}$$

where U_p is the Baum & McCaffrey's plume centerline velocity.

The Baum & McCaffery plume model predicts that, for a fire of total heat release rate $\dot{Q}_0$, any given height z of the plume is associated with some plume velocity U_p. In the case of a non–combusting spherical particle, released from a certain height z= z_0 at which it experiences no acceleration, Equation 9 is

$$0 = \frac{1}{m_p} C_D \rho_a A U_p^2 - g. \tag{10}$$

If z_0 lies in Region I of the plume (Figure 1a) then substituting $U_p = 2.18\, U_c \sqrt{z/z_c}$ for U_p into Equation 10 gives

$$z_0 = \Big(\frac{1}{2.18^2} \frac{z_c}{U_c^2} \frac{4}{3} \frac{g\, d_p\, \rho_p}{C_D\, \rho_a}\Big). \tag{11}$$

Height z_0 is the minimum loftable height, and the expression suggests that, given a spherical particle with diameter d_p and density ρ_p, there exists a unique height z_0 within Region I below which a fire of heat release rate $\dot{Q}_0$ is unable to loft the particle.

Substituting U_p= $3.64\, U_c\, (z/z_c)^{-1/3}$ for Region III of the plume into Equation 10 and solving for z= z_{max} gives,

$$z_{max} = \Big(\frac{3\, C_D\, \rho_a\, 3.64^2}{4\, d\, \rho_s\, g}\Big)^{3/2} z_c. \tag{12}$$

Here z_{max} is the maximum height that a lofted particle of given size can attain.

The maximum loftable diameter $d_{0,max}$ of a particle of given density is obtained by substituting U_p = $2.45\, U_c$ (Region II) into Equation 10. Solving for d= $d_{0,max}$ gives

$$d_{0,max} = \frac{3\, \rho_s\, C_D}{4\, \rho_a\, g} \big(2.45\, U_c\big)^2. \tag{13}$$

Figure 1b shows the plot of minimum loftable height z_0 as a function of particle size d_p in the case of a fire with $\dot{Q}_0$= 5.0 MW and particle density ρ_p= 513 kg m^{-3} (Bhutia et al., 2009).

Using a fourth–order Runge Kutta (RK4) scheme, the equation governing the (x,y,z,t) position of a particle (Bhutia et al., 2009) and Equation 9 were numerically integrated to first solve for the trajectories of spherical non–burning particles released above Baum & McCaffrey's stationary pool fire. Here (x,y,z,t) have the usual definitions. A constant time step of 0.01 s was used. For test purposes, four particles with diameters d_p= 5, 10, 20, and 25 mm were released at their corresponding minimum loftable heights of 0.8538, 1.7076, 3.4152, and 4.269 m, respectively. Particles of d_p less than 5 mm were not chosen because particles of this small size burn completely in air before landing. Larger spherical (i.e., with no lift or glide) particles tend to have too short a flight time resulting in short spotting distances. All firebrands were given a slight perturbation in the upward direction upon release. Once released, the only motion was in the vertical direction driven by the buoyant plume.

Figure 2a,b illustrates the potential of Baum & McCaffrey's Plume Model's to loft non–burning particles. The curves in the figure show that the lighter particles gain height faster than the heavier ones. Figure 2b illustrates the vertical velocity profile of the particles. A particle of a given size, upon release from an initial minimum loftable height z_0, accelerates in Region I of the plume. Particle acceleration slows on entering Region II, and by the time a particle reaches Region III, gravity force overtakes the drag force and the particle starts decelerating.

Repeating the RK4 solution, and including equations representing the effective mass diameter in firebrand combustion and the time rate of change of temperature for a spherical firebrand particle (Bhutia et al., 2009), the results for burning spheres were obtained and are illustrated in Figure 2c,d. Figure 2c shows the vertical propagation of the firebrands as a function of height. In comparison to non–burning particles, firebrands gain more height at a faster rate. This is explained by the fact that a burning particle is constantly losing mass as it burns. Although the smaller particles are gaining height quickly, at the same time they are combusting at a faster rate compared to the larger particles. This is expected as the burning rate constant β increases with the magnitude of the relative velocity $\vec{V}_r$ of the particle. The plus symbols on the path of the firebrands in Figure 2c denote the points on the paths beyond which particle combustion ceases. This occurs when the ratio $m_p/m_{p,0}$ reduces to 0.24 (Bhutia et al., 2009). The particle then begins to cool from its ignition temperature of 973 K (Bhutia et al., 2009). This is shown in Figure 3.

Here the potential of a background windfield typical of operational firebrand prediction to propagate the four plume–lofted test particles is investigated. The expression used to generate the background wind field is

$$|[U,V,W]| = \Big[\frac{v_*}{\kappa}\ln\Big(\frac{z}{z_{0_*}}\Big), 0, 0, \Big]. \qquad (14)$$

The v_* is the friction velocity, defined as the square root of the ratio of the surface stress to density of air, κ is the Von Karman's constant, and z_{0_*} is the surface roughness length, which is a measure of the surface vegetation height. The $[U,V,W]$ represents [x,y,z] wind components. Figure 4 (left panels) shows the vertical profile of the background wind field determined by Equation 14, where v_*= 0.7 m s^{-1}, κ= 0.4, and z_{0_*} = 0.05 m for uncut grass. All particles were released at rest from a height of 50 m above the ground.

Using the RK4 scheme, the equations governing the time rate of change of temperature for a spherical firebrand particle (Bhutia et al., 2009) and 9 were again numerically integrated, and Figure 4a (right panel) shows the trajectories of the four non-burning test particles. The result indicates that the horizontal propagation distance of non–burning particles is sensitive to particle size, with the smallest particle traversing the maximum downwind distance. A comparison of propagation distances shows that non-combusting particles (Figure 4a) traverse further than combusting particles (Figure 4b).

In the absence of lift, a particle's vertical motion is a consequence of the imbalance between the force of gravity F_g and the vertical drag force $F_{D,z}$. At the instant a non-combusting particle is released at rest at a certain height, the motion is driven solely by gravity. The moment the particles start falling, the drag force starts opposing the motion (Figure 5). As illustrated in Figure 5b, for a non–combusting particle, the drag force grows quickly to match the force of gravity. The particle then begins to fall with a constant vertical velocity known as the terminal or settling velocity V_t (Figure 5d; blue triangles) that is characteristic of a particle's given size, weight, and air density. The expression for the terminal velocity of a particle is

$$V_t = \sqrt{\frac{2\,m_p\,g}{\rho_a\,A\,C_D}}, \qquad (15)$$

and in the case of a spherical particle is

$$V_t = \sqrt{\frac{\rho_p\,d_p\,g}{3\,\rho_a\,C_D}}. \qquad (16)$$

A firebrand is losing volume and consequently mass. As the volume reduces, F_g reduces too and consequently $F_{D,z}$. Since F_g is proportional to cube of the

radius and $F_{D,z}$ to square of the radius, it might be expected that F_g decreases faster than $F_{D,z}$. But, F_{D_z} cannot exceed F_g, so the adjustment is made through a decrease in terminal velocity V_t, which explains the decrease in Figure 5d (red squares) in the $V_{p,z}$ of a burning particle after its initial rise.

The ρ_a around the particle was calculated at an average of air (20 °C) and flame (700 °C) temperatures, which decreases ρ_a from 1.204 to 0.55 kg m^{-3}. This change is so significant that the burning particles attain a higher initial terminal velocity relative to non–burning particles, as seen in Figure 5d.

The results indicate that although the lighter particles are lofted at lower heights and gain height at a faster rate, at the same time they are burning at a higher rate, consequently losing mass and volume at a faster rate. While heavier particles are lofted only at greater heights and the gain in height is very negligible, they burn for a longer period of time at a slower rate. The results also suggest that the combustion has a significant influence on the propagation distance of spherical particles. Burning particles are shown to traverse a shorter distance relative to non–burning particles. However, both lofting heights and propagation distances are found to be sensitive to particle size. The smaller the particle, the greater the downwind distance traveled. The smaller the particle, the greater the gain in height.

2. A Coupled Wildfire–Atmosphere Wind Field

Here (Sun et al., 2009)'s coupled fire/atmosphere UU-LES (University of Utah's Large Eddy Simulator) simulations are used to represent the evolution of a wildland grass fire in a convectively–driven atmospheric boundary layer (CBL). To study the differences in the spread of grass fires in dry convectively–driven ABLs, Sun et al. (2009) performed coupled wildfire UU–LES simulations of moving grass fires, burning in uniform fuel on level terrain, initialized as straight line fires perpendicular to the background mean wind direction. The initial ABL conditions in the CBL simulations were a constant with height, mean westerly wind of 5.5 m s^{-1}, a boundary layer depth of approximately 1000 m, and a constant surface heat flux of 0.24 W m^{-2}. Readers are referred to Sun et al. (2009) for details.

A CBL's primary flow structure is determined by a few large eddies driven by powerful updrafts. The scale of the eddies that dominates the simulated CBL was prescribed by the convective velocity scale (Deardorff, 1972), a function of the boundary layer depth and surface heat flux, and an estimate of the strength of the largest turbulent eddies in a CBL. The convective velocity scale for Sun et al. (2009)'s CBL simulations was $\sim$ 2.0 m s^{-1}. After the CBL reached a quasi–steady state, but prior to the setting of fires, the largest variances of U, V, and W wind components in the UU-LES domain were similar in magnitude to the convective velocity scale.

Sun et al. (2009) then ignited multiple fire lines, initially identical in size (20 m in length) and heat release rate (10^5 W m^{-2}), at different locations in the UU-LES simulated CBL. For the rest of the study, when examining the impact of fire–induced and CBL turbulence in the flow on the lofting and propagating of fire particles, model winds from the faster spreading fire line in Sun et al. (2009)'s 10-minute coupled UU-LES grassfire simulation are used.

Figure 6 shows the general differences between the vertical plume flow fields determined by Baum and McCaffery's model and Sun et al's moving grass fire in a CBL. The rate of heat release for Sun et al's CBL fire ranged from 1 to 6 $\times 10^5$ W m^{-2}, while the rate of heat release from Baum and McCaffery's stationary fire remained constant at 10^5 W m^{-2}.

The updrafts and downdrafts associated with the interaction of fire–induced circulations and eddy circulations in a CBL ABL are important to fire evolution and spread (Sun et al., 2009). Figure 6a shows that for the coupled UU-LES, the mean W remains negligible and the variances of W constitute a fire plume's vertical velocity. Fire convection produces strong vertical motion, and the magnitude of the variances in W grows larger with height. The coupled UU-LES can provide both the mean and fluctuations in fields above a moving ABL-fire. The Baum and McCaffery model can only represent a fire plume in terms of single time–averaged mean fields above a stationary fire. Figure 6a shows the Baum and McCaffery model over estimating mean vertical plume velocity, particularly in the region immediately above the fuel bed in the combustion zone. Even the shape of the vertical velocity profiles of the coupled UU-LES and the Baum and McCaffery model are a complete mismatch.

Horizontal cross–sections of W at various heights above the ground for Sun et al's fast-moving fire (not given) show that the maximum updraft velocity increased from 3 m s^{-1} at a height of 10.5 m to 10 m s^{-1} at a height of 72 m. Vertical cross–sections (not given) show that the fire plume reached the top of the ABL ($\sim$ 1000 m) and was, under the influence of the turbulent flow and a westerly mean background wind, bent downwind and lacking a well–defined structure on the downwind side where brands are likely to exit the plume. The fire plume could not be described as Gaussian shaped. A representation of these features is important to spotting by firebrands because, as the following Section shows, the behavior of fire brands de-

pends heavily on the these wind conditions. The Baum and McCaffrey representation of plume velocity fails to depict any of these features.

Figure 6b,c compares the vertical variation of the horizontal flow field for Sun et al's moving grass fire with the steady mean logarithmic background wind domain provided by Equation 14 and used to represent the horizontal flow field in and around the Baum and McCaffrey stationary fire. In the UU-LES CBL domain a background east-west wind of 5.5 m s^{-1} and constant with height was used. Figure 6b shows that, except for some slight variance, this constant-with-height mean wind of 5.5 m s^{-1} is maintained over the UU-LES CBL fire. Figure 6c shows that the mean V and its variance remain small. Figure 6b,c shows the Baum and McCaffery model (dotted red lines) underestimating mean U, especially at the surface, and overestimating mean V, particularly in the region immediately above the fuel bed in the combustion zone.

3. Behavior and propagation of fire brands in a coupled fire/atmosphere wind field

Sets of numerical experiments were conducted to observe the influence of the fire–induced circulations and eddies in the coupled UU–LES CBL on the trajectories of combusting and non-combusting spherical particles. For each experiment $N_p = 45$ spherical particles were released at height Z_{rel} above ground level from points on a mesh of dimensions (80 m, 80 m) in the (x, y) directions. Mesh points were located 4 m apart in the x direction and 10 m apart in the y direction. The mesh was positioned so that it is centred over the strongest updraft region of the fire. Spherical particles of density ρ_p= 200 kg m^{-3} and diameter d_p= 20 mm were used. The value of d_p is not representative of grass embers or any specific wooden material. The combustion characteristics of the wood particles that were used are given in Bhutia et al. (2009). The mass–loss rate and diameter regression rate of a combusting particle are as described in Bhutia et al. (2009).

The coupled UU-LES wind field data from the simulations carried out by Sun et al. (2009) were captured at 20 s intervals. A weighted–mean linear temporal interpolation was used to reduce the time step from 20 s to the smaller time step of 0.625 s, suitable for a RK4 solution. Also wind values at the reduced time step, needed between model grid points, were obtained by weighted–mean linear spatial interpolation. Using these winds, the equations governing the motion of the firebrands were integrated numerically with the RK4 scheme.

Figure 9a shows the paths taken by non–combusting particles released from heights Z_{rel}= 30, 50, and 75 m. The figure provides an estimate of the downwind distance traversed by individual particles and the sensitivity of particle propagation to release height. The figure shows the higher the release height, the further the downwind distance traversed. This is attributed primarily to the fact that particles released at higher heights have more distance to travel before reaching the ground and in the process travel further downwind. But there are differences in propagation distance even among particles released at the same height. Figure 9a shows that particles with a wavy path have a longer flight time, and the wavyness in the path increases with particle release height. As seen previously in Figure 6, fluctuations in vertical plume velocity and fire–induced circulations increase with plume height, and the effects of this are reflected in the paths traversed by particles released at varying heights. Particles released higher up in the plume are caught in fire–induced circulations and taken further downstream. The shorter trajectories of particles released at lower heights suggest that these particles moved through the plume without significant deviation from a parabolic–like flight path.

Figure 9b is a x-y cross sectional view of the positions of the particles shown in Figure 9a. The figure shows the initial (t= 0 s) and final (t= 40 s) particle positions in the horizontal plane. On average downwind (x direction) propagation is larger than lateral (y direction) propagation in this ABL flow. With an increase in Z_{rel}, the particles's final positions lose resemblance to the initial rectangular horizontal mesh pattern. This suggests that, in addition to CBL turbulence, fire–induced circulations in and downstream of the plume cause particles to deviate significantly from a simple parabolic trajectory. Consequently the particles eventually lack a similar and distinct direction of motion or flight path. There is significant scatter or randomness to the propagation pattern, making the prediction of firebrand spotting even more uncertain. This important feature is not reflected by simpler two-dimensional de-coupled modelling of the phenomenon seen previously in Figure 4. Current operational models for spotting are not able to provide a propagation pattern like this, and it is possible that these models do not always predict the worst case scenario for spread of wildland fire by spotting.

Albini (1983) stressed the importance of fire–plume generated turbulence on initial firebrand momentum. Then lacking a numerical modeling approach similar to the UU-LES, Albini (1983) suggested the use of a power spectral density function to imitate the intensity and randomness of turbulence created by the fire at initial particle brand release. Here this approach is examined to determine if it is sufficient or even necessary for accurate prediction of firebrand propagation.

A set of numerical experiments were conducted in which random velocity magnitudes and directions are assigned to individual particles upon release inside the plume. The impact of initial momentum at particle release compared to the impact of fire–induced and CBL turbulence in the flow modeled by the coupled UU-LES approach on particle propagation was then investigated.

Four runs were conducted where N_p= 45 particles were released from a single height of Z_{rel}= 50 m. In the first run, E1, the particles were released from rest. In the second run, E2, random values ranging between 0.0 and 0.1 m s^{-1} were assigned to each particle's velocity components at release. This means that not only were the velocity components assigned random values but also directions. In the third run, E3, initial particle velocities were varied randomly between 0.0 and 5.0 m s^{-1}. And in the last run, E4, the initial particle velocities were varied randomly between 0 and 10.0 m s^{-1}. This final range of initial momentum is based on the maximum magnitudes of the fire–induced vertical wind velocities typically produced by a coupled UU-LES fireline and shown in Section 2.

Figure 8 show the estimates of the trajectories and downwind distances traversed by each particle released in experiments E1, E2, E3, and E4. Although there is a tendency for particles in E4 to take a longer flight path than particles in E1 (Figure 8a), the results show how relatively little impact initial momentum in the range of 0 and 10.0 m s^{-1} has on firebrand propagation (Figure 8b). The positions of particles at t= 30 s suggest that the particles with a randomly higher initial release velocity do traverse further, but the difference in path length is not large, while the scatter in particle positions is. A similar plot for E1 and E4 only (not given) indicates that the distances traversed by particles in the coupled UU-LES CBL wind field are not particularly sensitive to fluctuations in initial momentum. The results demonstrate that particle motion is governed mainly by fire–induced winds and flow turbulence, irrespective of the initial particle momentum, at least for an initial momentum of magnitude less than 10 m s^{-1}.

Here the effect of combustion versus no combustion on the flight paths of individual particles is examined. Figure 7 show the paths for each type when released from Z_{rel}= 50 m. Combusting particles are seen to fall faster to the ground in comparison to non-combusting particles (Figure 7a). Whereas particle flight paths appear to be relatively insensitive to fluctuations in initial particle momentum, Figure 7 shows that the flight paths of combusting particles are consistently and significantly shorter than non-combusting particles. Figure 7b indicates that the amount of scatter in particle positions is equally significant in each case and not a function of initial particle momentum or combustion.

4. Concluding Remarks

This study shows several ways that the current operational modeling approach to firebrand transport is limited in its usefulness as a predictor of ignition by spotting. It is not equipped to handle the typically different and changing ABL and complex fire/atmosphere interactions. Firebrand motion is governed primarily by the wind field surrounding it, and a complete three-dimensional time–varying representation of the fire/atmosphere flow is of critical importance for accurate prediction of firebrand propagation.

Firebrand propagation is sensitive to release height. The higher the release height, the further the downwind distance traversed. For the environmental ABL conditions used in this study, the downwind motion of particles is driven mainly by the mean wind component, the lateral motion by the fire–induced fluctuations. The wavelike character of the early lateral displacement of particles suggests that the initial paths of the particles are in the fire–induced circulations.

Firebrand propagation is also sensitive to combustion. Burning particles tend to fall faster to the ground in comparison to non-burning particles, and the differences in trajectories of combusting versus non–combusting particles are significant. Accurate operational firebrand propagation prediction requires particle combustion modeling.

Firebrand propagation is relatively insensitive to initial particle momentum. Even an assignment of varying randomness to the initial velocity of brand particles does not influence the motion in comparison to the influence of the turbulent flow created by the coupling between the fire and the ABL flow. This approach is therefore ineffective when used in simple de-coupled empirically–based classical plume models to emulate in–plume fire–induced turbulence.

A simple empirically–based classical plume approach to modeling firebrand trajectory may not predict the worst case scenario for fire spotting. There was a great deal of scatter in particle location when released from the coupled UU-LES dynamically–modeled fire plume interacting with a convectively–active ABL.

Finally, in every case, as firebrands are translated downwind of the fire, the fire-induced convection and CBL winds cause significant randomness in particle motion. Fire spotting by brands is not deterministic in the ABL and a probabilistic prediction method is warranted.

ACKNOWLEDGMENTS. Mr. Sangay Bhutia's re-

search was supported by Canada's National Science and Engineering Research Council's Joint Infrastructure Interdependencies Research Grant Program. Dr. R. Sun's research was supported by the United States Department of Agriculture Forest Service Research Joint Venture Agreement 03-JV-11231300-08 while at the University of Utah, Department of Atmospheric Sciences. A gratis grant of computer time from the Center for High Performance Computing, University of Utah, is gratefully acknowledged.

References

Albini, F. A., 1983: Transport of firebrands by line thermals. *Combustion Science and Technology*, **32**, 277–288.

Alexander, M. E., C. Tymstra, and K. W. Frederick, 2004: Incorporating breaching and spotting considerations into PROMETHEUS, the Canadian wildland fire growth model (Chisholm/Dogrib Fire Research Initiative). Technical Report Quicknote 6, Foothills Model Forest, Hinton, Alberta, Canada.

Baum, H., and B. McCaffrey, 1989: Fire induced flow field theory and experiment. *Proceedings of the Second International Symposium*, Fire Safety Science.

Bhutia, S., M. A. Jenkins, and R. Sun, 2009: The importance of fire/atmosphere coupling and boundary-layer turbulence on firebrand propagation. *Submitted to J. of Advances in Modeling Earth Systems*.

Deardorff, J. W., 1972: Numerical investigation of neutral and unstable planetary boundary layers. *J. Atmos. Sci.*, **29**, 91–115.

McCaffrey, B., 1983: Momentum implications for buoyant diffusion flames. *Combustion and Flames*, **52**, 149–167.

Sun, R., S. K. Krueger, M. A. Jenkins, and J. J. Charney, 2009: The importance of fire/atmosphere coupling and boundary layer turbulence to wildfire spread. **18**, 50–60.

Tse, S. D., and A. C. Fernandez-Pello, 1998: On the flight paths of metal particles and embers generated by power lines in high winds — a potential source of wildland fires. *Fire Safety Journal*, **30**, 333–356.

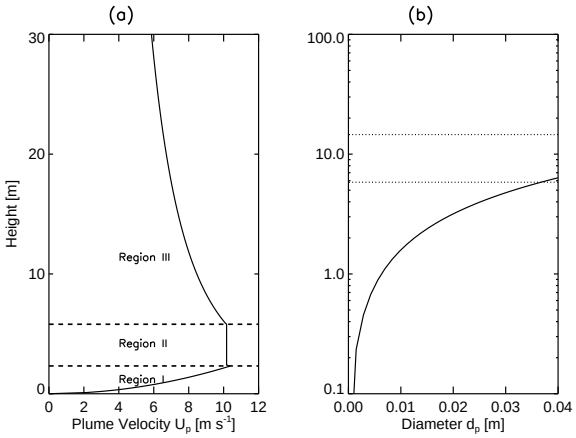

Figure 1: Vertical profiles of (a) central vertical plume velocity U_p and (b) minimum loftable height z_0 as functions of particle size d_p. Dotted lines separate Regions I, II, and III of the plume. Results are based on the Baum and McCaffrey's plume model.

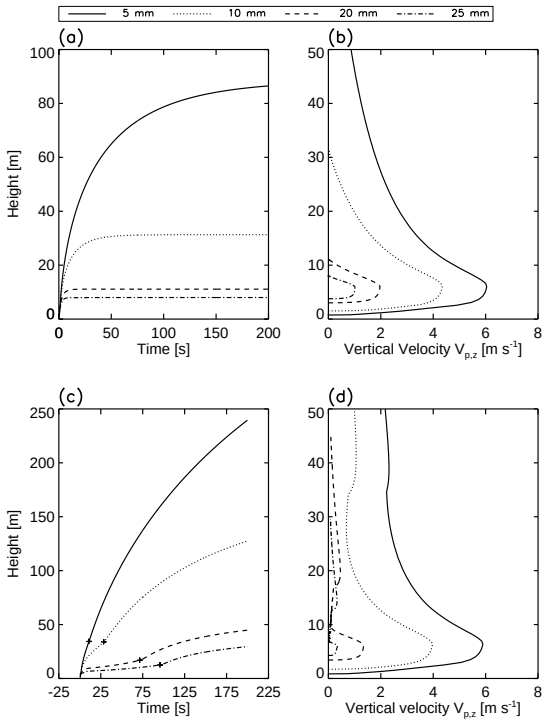

Figure 2: Vertical profiles of (a) lofting heights z and (b) vertical velocity $V_{p,z}$ of non–burning particles, and (c) lofting heights z and (d) vertical velocity $V_{p,z}$ of burning particles. Particle diameters d_p= 5, 10, 20, and 25 mm. Results are based on the Baum and McCaffrey's plume model.

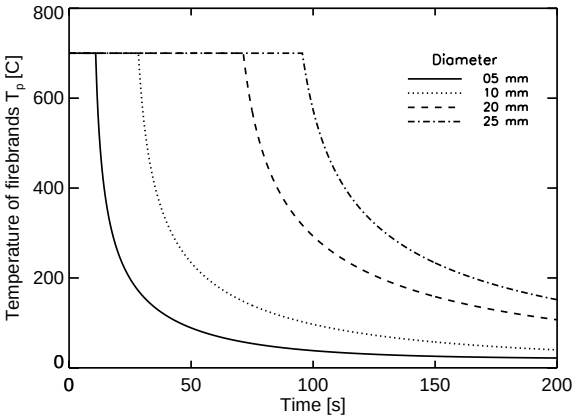

Figure 3: As in Figure 2, except for T_p, temperature of burning firebrands, as a function of time.

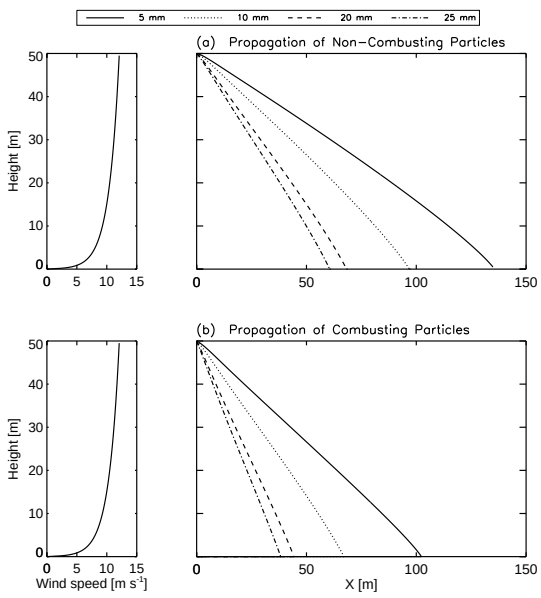

Figure 4: Trajectories of (a) non–combusting and (b) combusting particles of diameters d_p= 5, 10, 20 and 25 mm, released from rest with Z_{rel} = 50 mm and vertical velocity $V_{p,z}$= 0 m s^{-1}, in a steady background east-west wind field with a logarithmic vertical velocity profile (left panels) determined by Equation 14. Results are based on the Baum and McCaffrey's plume model.

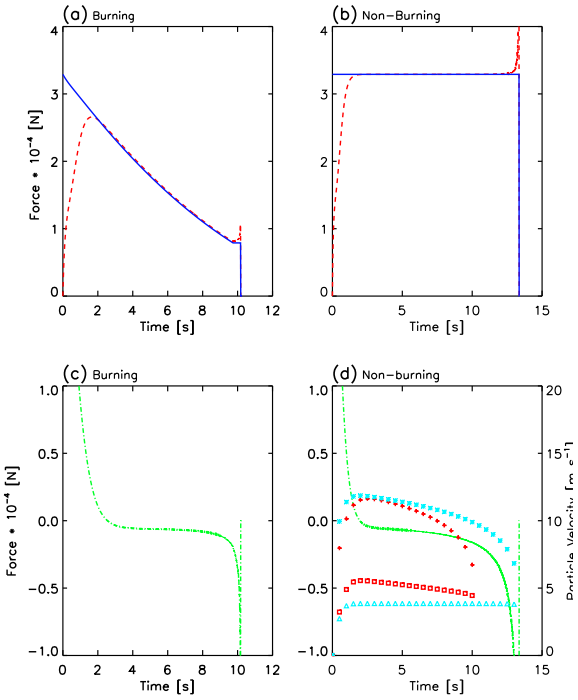

Figure 5: The vertical drag and gravitational force as functions of time for (a) burning and (b) non–burning particles, and the horizontal drag for (c) burning and (d) non–burning particles, as functions of time. Also plotted as functions of time are the (d) downwind velocity $U_{p,x}$ [m s^{-1}] (plus signs and stars) and vertical velocity $V_{p,z}$ [m s^{-1}] (squares and triangles) of combusting (red) and non-combusting (blue) particles. Results are based on the Baum and McCaffrey's plume model.

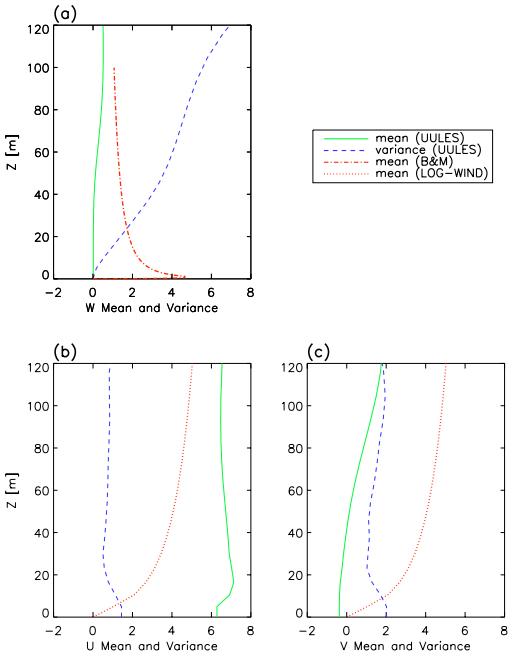

Figure 6: Vertical profiles of mean and variance of wind components (a) W, (b) U, and (c) V. Solid green and dashed blue lines represent results from the fire–induced CBL UU-LES wind field and dotted red lines represent the wind result of Baum and McCaffrey's plume model.

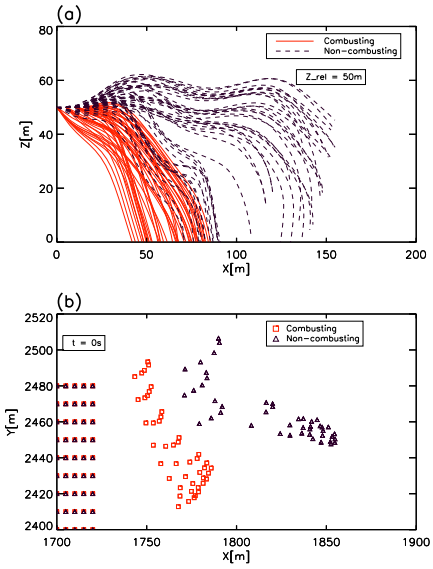

Figure 7: Plot (a) is x–z cross section showing paths taken by combusting particles (solid red lines) and non–combusting particles (dashed black lines) at t= 30 s after release. Plot (b) shows x–y positions of combusting (red squares) and non-combusting particles (black triangles) at t = 0 s and at t = 30 s after release.

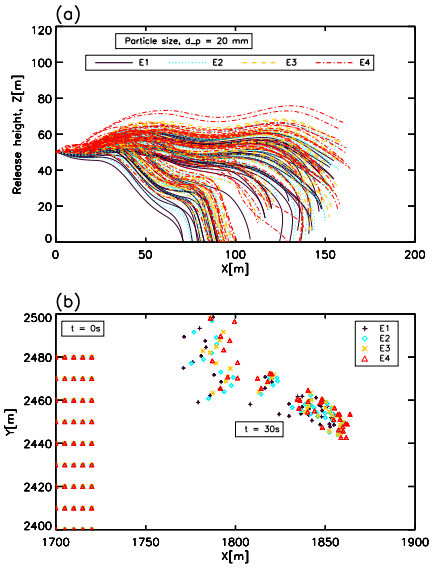

Figure 8: For runs E1, E2, E3, and E4, with release height Z_{rel}= 50 m, plot (a) is x–z cross section showing paths of non–combusting particles and plot (b) shows x–y positions of particles at t= 0 s and t= 30 s after release.

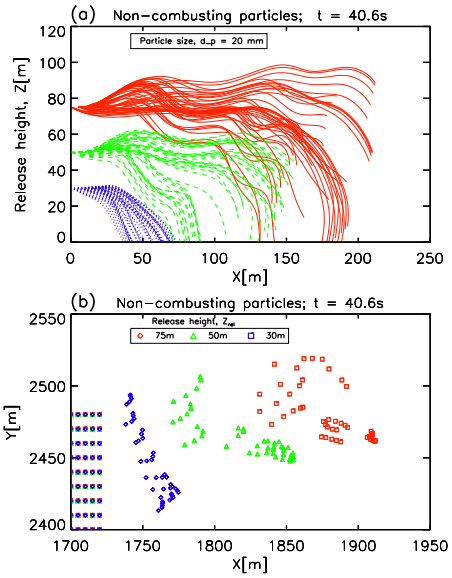

Figure 9: Plot (a) shows paths of non–combusting particles with release heights Z_{rel}= 75 m (red solid lines), 50 m (green dashed lines), and 30 m (blue dotted lines). Plot (b) shows positions of the particles in the horizontal (x–y) plane at t= 0 s and t= 40 s after release. All particles were released from rest.

Table 1: Plume Correlation Parameters*

Region	Range	n	A	B
Flame (Region I)	$0 \leq z^* \leq 1.32$	1/2	2.18	2.91
Intermittent (Region II)	$1.32 < z^* < 3.30$	0	2.45	3.81
Plume (Region III)	$3.3 \leq z^*$	-1/3	3.64	8.41

* based on Baum and McCaffrey (1989) and McCaffrey (1983)